Long-Term Testing of a High Temperature Polymer Electrolyte Membrane Fuel Cell: The Effect of Reactant Gases

F. Javier Pinar, Nadine Pilinski, and Peter Wagner
NEXT ENERGY. EWE Research Centre for Energy Technology at the University of Oldenburg, Carl-von-Ossietzky Str. 15, 26129 Oldenburg, Germany

DOI 10.1002/aic.15044
Published online October 1, 2015 in Wiley Online Library (wileyonlinelibrary.com)

The investigations have been conducted with different oxidants and fuels with the aim of determining the state-of-the-art of commercially available high temperature polymer electrolyte fuel cells based on polybenzimidazole for its application in combined heat and power generation systems. The fuel cell test performed with synthetic reformate (−63 μV/h) showed an increase of anode charge and mass transfer resistances. This behavior has suggested that CO may be generated from the CO_2 included in the synthetic reformate via reverse water gas shift reaction. The fuel cell test performed with pure O_2 developed the highest degradation rates (−70 μV/h) due to fast oxidative degradation of membrane electrode assembly materials such as cathode catalyst and membrane. Fuel cell operation with H_2/air exhibited the lowest degradation rates (−57 μV/h) and it requires longer investigating times to identify the different degradation mechanisms. Moreover, fuel cell tests performed with air suggested longer break-in procedures to complete catalyst activation and redistribution of electrolyte. © 2015 American Institute of Chemical Engineers *AIChE J*, 62: 217–227, 2016
Keywords: electrochemical engineering, fuel cell, high temperature polymer electrolyte fuel cells, polybenzimidazole, long-term testing, synthetic reformate, commercial membrane electrode assembly

Introduction

High temperature polymer electrolyte fuel cells (HT-PEMFC) are gaining more attention of fuel cell research groups due to their desired features for combined heat and power generation systems (CHP).[1,2] HT-PEMFCs are able to operate between 120 and 180°C, whereas their main competitors, low temperature (LT-) PEMFC operate below 100°C. The higher operation range of HT-PEMFC respect to LT-PEMFC reflects some benefits. Among all of the HT-PEMFC features better fuel impurities tolerance, no liquid water phase and improved generated heat utilization regarding to LT-PEMFC can be highlighted.[3–6] Phosphoric acid doped polybenzimidazole (PBI) is becoming the standard electrolyte material for this kind of HT-PEM technology. PBI shows good proton conductivity, virtually zero electro-osmotic drag coefficient, and good thermal, chemical, and strain resistances.[7–10] However, the bottle neck of PBI technology is its higher degradation rate compared to Nafion® technology with LT-PEMFC. The different materials that form the hardware of a HT-PEMFC are exposed to a higher acidic environment, higher temperatures up to 180°C and higher electric potentials than Nafion® based LT-PEM systems. Such operating conditions are the main reasons for faster degradation. Fuel cell targets for stationary applications (HT- and LT-PEM) vary from 40,000 to 90,000 h of operation.[11–13] Long-term testing in PBI-based HT-PEMFC technology has already reached more than 17,000 h of operation.[14–16] Nevertheless, PBI-based HT-PEMFC technology lifetime must be further improved to reach the desired durability targets.

The membrane electrode assembly (MEA) as the core of the fuel cell is a complex structure composed of various materials. During long-term operation, all the MEA components are susceptible to physical, chemical, and electrochemical degradation that summarizes into overall fuel cell electrical efficiency reduction. There are many causes for failures within the components, and each of them contributes to the performance reduction. Besides, these degradation effects also interact with each other resulting in a much more complex interpretation and understanding of ageing processes. For example, the electrical conductivity is influenced through carbon corrosion as well as the hydrophobicity of the gas diffusion electrode (GDE).[14,17] In LT-PEMFCs, the hydrophobicity depletion is associated to generate mass transfer limitations as produced water may fill partially the porous structure of the GDE. Moreover, catalyst detachment is also associated to carbon corrosion that leads to catalytic activity reduction.[12]

Operation conditions such as temperature, backpressure or partial pressure of reactant gases may also limit the fuel cell lifetime. Hydrogen from reformate instead of pure hydrogen as anode feed could generate anode mass transfer losses to the catalyst active sites.[18] Hydrogen dilution in reformate could also cause fuel starvation in some regions of the catalyst surface that turns to faster anode catalyst degradation over time.[19–21] Moreover, the different reformate components (CO_2, CO, CH_4, H_2O, etc.), that accompany the hydrogen, could also reduce fuel cell lifetime owing to side reactions that lead to fuel cell materials deterioration such as catalyst poisoning or carbon corrosion.[22,23] Pure oxygen instead

Correspondence concerning this article should be addressed to F. J. Pinar at javier.pinar@next-energy.de.

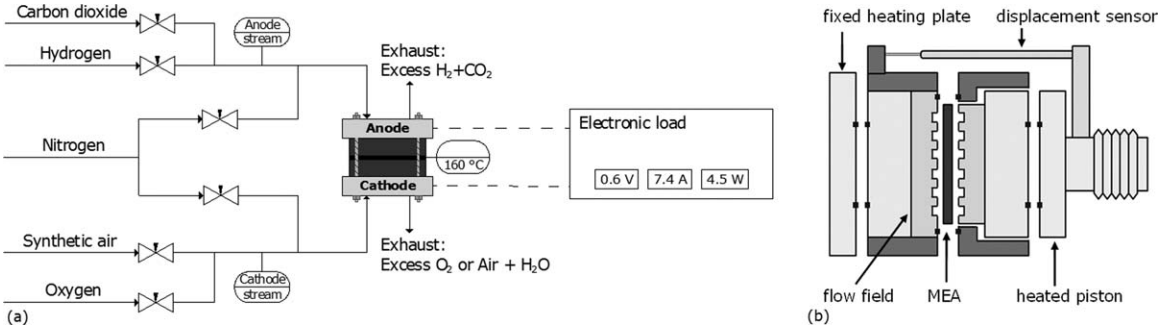

Figure 1. Schematic representation of (a) experimental set-up and (b) cell compression unit.

of air as cathode inlet will reduce mass transfer losses considerably. The cathode electrode is quite sensitive to oxygen concentration and oxygen reduction reaction (ORR) would be improved.[24] On the contrary, larger fuel cell performance reduction over time is expected with pure oxygen operation as MEA materials are exposed to a higher oxidative environment.[12]

The present work is under the work plan of the European Project CISTEM which is supported by the Fuel Cell and Hydrogen Joint Undertaking (FCH-JU grant agreement no. 325262). The purpose of the CISTEM project is to proof the viability of HT-PEMFC technology for mini CHP systems up to 100 kW_{el} power. One of the key points of this project is to improve the electrical efficiency of the HT-PEMFC CHP system. The operation strategy to reach this objective is utilizing an electrolyser where hydrogen and oxygen are produced from water. The utilization of oxygen from an electrolyser, which is normally wasted, may improve the electrical efficiency as well as performance of the fuel cell considerably. Moreover, the CHP system is designed to be fuel flexible. Therefore, the HT-PEMFC must allow the operation with impurity contaminated hydrogen from natural gas reforming as well as pure hydrogen from water electrolysis. Therefore, the scope of the present work is to determine the effect of reactant gases on the fuel cell performance and the possible degradation over time due to higher oxygen partial pressures in the cathode in comparison to operation with air as well as lower hydrogen partial pressures in the anode in comparison to operation with pure hydrogen. Thus, three long-term tests at constant load conditions have been performed with different cathode and anode reactants compositions. Moreover, the tested MEAs have been electrochemically characterized using different electrochemical techniques such as electrochemical impedance spectroscopy (EIS), polarization curves and linear sweep voltammetry (LSV). Thus, the selected MEA characterization methods allow identification and classification of the different mechanisms that may influence the degradation of the MEAs under investigation as for example, catalyst active surface reduction, hydrogen crossover enhancement, short circuit formation, and/or proton transfer deterioration in the membrane over time.

Experimental

Membrane electrode assembly

Dapozol®-G55 MEAs were delivered by Danish Power Systems (Denmark) with a nominal active surface area of 25 cm^2. This type of MEA utilizes a phosphoric acid doped m-PBI as membrane polymer electrolyte and nonwoven carbon cloth as gas diffusion layer (GDL) material in the electrodes. The acid content of this type of MEA is ~8 to 9 H_3PO_4 molecules per monomer of PBI. Further information cannot be given due to proprietary issues.

Cell compression units and fuel cell test benches

Pragma Industries (France) and Baltic Fuel Cells (Germany) cell compression units (CCU), designed for single cell operation, have been utilized for these experiments. Both systems allow the compression force transmission from a piston directly on the active surface area of the MEA. Displacement sensors on the CCUs enable recording of MEA thickness changes during the long-term tests. On the one hand, the fuel cell was set up with fivefold serpentine flow field bipolar plates (BBP) for tests performed with air as oxidant. On the other hand, grid flow field BPPs were selected for the test performed with pure O_2 as oxidant. The nominal contact pressure applied to the MEAs during the experiments was 0.75 MPa for the fivefold serpentine flow field and 0.53 MPa for the grid flow field BPPs setup. The different nominal contact pressures are required by the different real land contact areas of the area of the BPPs. For the grid flow fields, the land area is almost 30% smaller (9.49 cm^2) in comparison to fivefold serpentine flow fields (13.35 cm^2).[25] By taking into account the different nominal contact pressures, all tests can be operated at constant contact pressure modes with an absolute contact pressure of 1.40 MPa. The selected real contact pressure is an optimized value that guarantees gas tightness as well as providing good electrical contact between MEA materials and BPPs without damaging the MEA.[26,27]

The Evaluator C50-LT test bench (FuelCon AG, Germany) operates the Pragma Industries CCU, whereas the Evaluator C1000-LT test bench (FuelCon AG, Germany) operates the Baltic Fuel Cells CCU. Constant stoichiometry conditions were selected for operation. Thus, anode supply was fixed with a stoichiometric factor of 1.5 for pure hydrogen and synthetic reformate operation (supplier recommendation). Cathode supply was fixed with a stoichiometric factor of 2 for synthetic air operation, whereas a stoichiometric factor of 9.5 was used for pure oxygen operation. The difference between the oxidant stoichiometries allowed same volume flows on the cathode side. The same volume flow strategy was followed in the anode side. The synthetic reformate gas mixture is controlled via mass flow controllers in the FC test bench which allows the same anode stoichiometric factors as well as volume flow rates like operation under pure H_2. The synthetic reformate gas composition was set to 78.1% mol H_2 and 21.9% mol CO_2 which was verified by gas chromatography with an error of ±0.5%.

A schematic representation of the experimental set-up and CCU can be found in Figure 1.

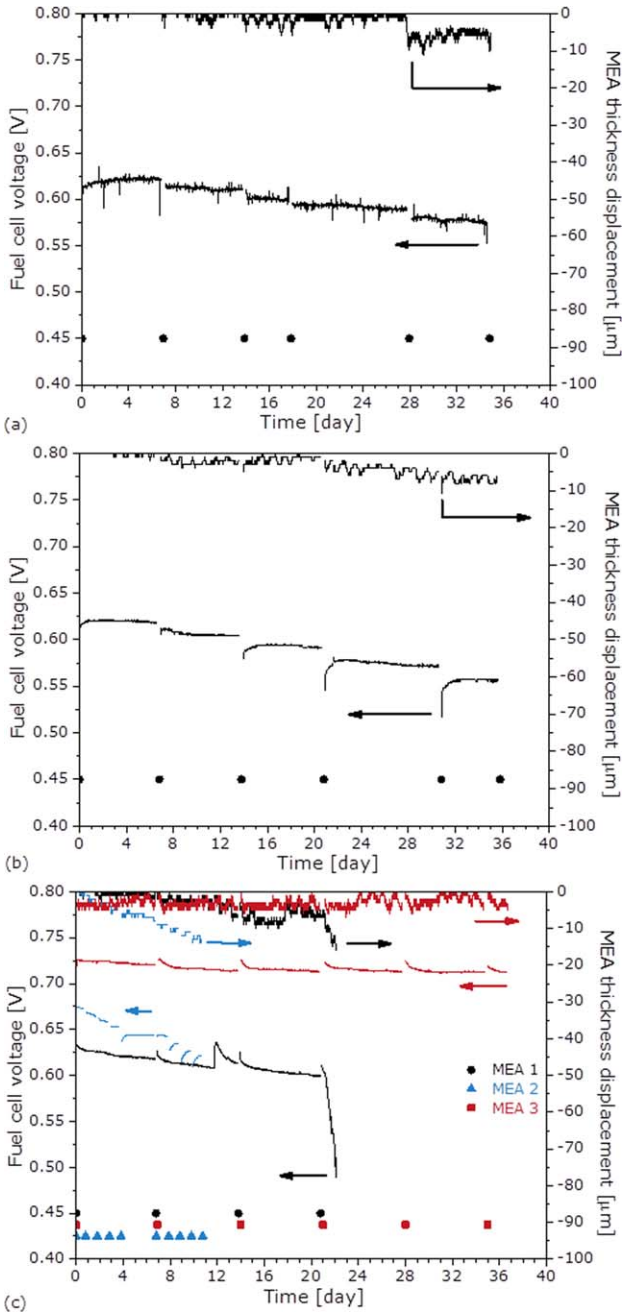

Figure 2. Fuel cell voltage over time for the fuel cell operating with (a) H_2/air ($\lambda_{anode}/\lambda_{cathode} = 1.5/2$), (b) 78% H_2 + 22% CO_2/air ($\lambda_{anode}/\lambda_{cathode} = 1.5/2$), (c) H_2/O_2 ($\lambda_{anode}/\lambda_{cathode} = 1.5/9.5$).

Current density was interrupted for MEA characterization on day: see black circles, red squares, and blue triangles. $T = 160°C$, $j = 0.3$ A/cm^2, $p = 0.1$ MPa, fivefold serpentine and grid flow field (MEA 1 in c), $P_{c,real} = 1.4$ MPa. [Color figure can be viewed in the online issue, which is available at wileyonlinelibrary.com.]

Electrochemical measurements and further experimental conditions

Three long-term tests at constant load conditions were performed with a duration of 1000 h each. The first test was performed with pure hydrogen and air, the second one has been performed with synthetic reformate and air, and the third one has been performed with pure hydrogen and oxygen.

The MEAs followed a specific break-in procedure given by Danish Power Systems. The fuel cell MEAs were mounted in a fixture and clamped with 1.3 N m torque. The fixture was installed into the compression unit and the break-in procedure started with heating the fuel cell up to 120°C under nitrogen before the fuel supply was turned on. In the presence of fuel, a current density of 0.3 A/cm^2 was applied to the MEA. Then, the cell was heated up to the final operating temperature of 160°C. Duration of break-in usually lasted between 50 and 100 h.

The electrochemical characterization procedures included besides polarization curves also EIS as well as LSV. An external potentiostat Modulab 2100A (Solartron Analytical, U.K.) was connected to perform EIS and LSV. EIS measurements were performed in the potentiostatic mode with the application of an alternating voltage with perturbation amplitude of 10 mV rms within the frequency range from 100 kHz to 100 mHz. For LSV measurements, nitrogen was passed through the cathode (working electrode) and hydrogen through the anode side (counter and pseudoreference electrode). The flow rates were 0.3/0.3 L/min for anode and cathode, respectively. The LSV scans were performed with a potential sweep between the initial rest potential and 0.5 V and a scan rate of 2 mV/s.

After break-in and complete initial electrochemical characterization, the MEA was continuously operated with a load of 0.3 A/cm^2. The constant load operation was interrupted once a week for polarization curves, EIS, and LSV measurements. On the starting day, the displacement sensor was set to 0 μm, and the displacement was also continuously recorded.

Results and Discussion

Fuel cell voltage over time

Figure 2 shows the results from the three 1000 h long-term tests performed at constant current density (0.3 A/cm^2). Break-in time is not shown for any of the three tests. This step is considered as an initial period of fuel cell operation that enables reproducibility and comparability of results for contaminant and performance investigations. During this first period of time, the MEA may undergo removal of impurities from the catalyst, ripening of the catalyst, redistribution of the electrolyte and membrane humidification.[28]

From Figure 2a (H_2/air) and Figure 2b (synthetic reformate/air), fuel cell voltage at 0.3 A/cm^2 has improved during the first week of the tests and then, fuel cell voltage reduction has been observed until the end of the test. On the contrary, MEA 1 Figure 2c (H_2/O_2) does not show the fuel cell voltage improvement during the first week as observed within the other two tests from Figures 2a,b. In this case, fuel cell voltage reduction over the whole test has been recorded. Moreover, this test has not reached the 1000 h of operation as it developed a large fuel cell performance reduction after the fourth week of characterization of the MEA. So the fuel cell test had to be stopped. At this point, two more long-term tests with other Danish Power Systems (DPS) MEAs have been included in Figure 2c for the fuel cell operating H_2/O_2 to understand the short lifetime of MEA 1. MEA 2 and MEA 3 are MEAs belonging to different batches than MEA 1 but have been operated with same flow field design and nominal contact pressure (absolute contact pressure of 1.40 MPa) than those tests shown in Figure 2a (H_2/air) and Figure 2b (synthetic reformate/air). It can be clearly observed that the three MEAs operated with H_2/O_2 (Figure 2c) have shown different behaviors.

Regardless the fuel or oxidant used the fuel cell voltage instability after MEA characterization has lasted little time until reaching steady values. This behavior could be due to restoration of adequate humidification in the fuel cell.[29] Then, the fuel cell voltage from MEA 1 and MEA 2 (Figure 2c) continued the previous voltage trend observed before MEA characterization while the other three MEAs tested have shown stepwise decreases in voltage. Operation with MEA 2 (Figure 2c) has been different than for the other tests shown as it was subjected to a daily characterization and further results are not shown owing to different operation routine. Nevertheless, the results presented in Figure 2c form MEA 2 can be used to highlight the impact of the used MEA characterization routine on fuel cell lifetime. The test performed with H_2/air has also shown the voltage stepwise decreases from one MEA characterization routine to next one but the impact of MEA characterization has been more severe to the test performed with synthetic reformate/air over time. In this case, the MEA characterization performed in day 7 of operation has developed a voltage reduction around 7 mV while voltage has been reduced 15 mV after MEA characterization in day 31. MEA characterization consisted of polarization curves, impedance spectroscopy measurement, cyclic and linear sweep voltammetries where voltage is mainly cycled from high to low values. Therefore, fuel cell performance reduction after MEA characterization may be a result of cathode electrode potential cycling. Darling et al.[30] presented a mathematical model of oxidation and dissolution of supported platinum catalyst in PEMFC during potential cycling and compared the kinetic expressions to available experimental data. They concluded that platinum oxidation/reduction occurred during cycling but concentration of platinum dissolution increased for higher sweep rates at high cathode potentials (~Open Circuit Voltage (OCV)) as platinum oxide surface equilibrium at high potentials is slow. Moreover, Jahnke et al.[31] has recently shown modeling about reversible and irreversible degradation in direct methanol fuel cells. The model describes irreversible loss of platinum active surface by particle growth due to dissolution/precipitation of platinum (Ostwald ripening) and coalescence, whereas describes reversible loss degradation by formation of platinum oxide. Thus, the model suggests the net platinum dissolution rate is proportional to the platinum surface which is not covered by the oxide layer.

MEA thickness also reduced over the whole test for all MEAs investigated. In the case of fuel cell operation with H_2/air and synthetic reformate/air, MEAs thickness was reduced 8–10 μm from their initial thickness in 35 days of operation, whereas MEA 1 and MEA 2 operated with H_2/O_2 has turned to 16 and 14 μm in 22 and 11 days of operation, respectively. Thus, pure O_2 operation revealed a high impact on degradation of MEA materials in MEA 1 and MEA 2 because the MEA thickness reduced twice as much than in the other two long-term tests operated with air. In contrast, MEA 3 from Figure 2c has shown similar trend but slight lower values (5 μm) than those MEAs operated with H_2/air and synthetic reformate/air. These reductions on the MEA thicknesses in long-term operation can be related to a summarized thinning of the MEA materials as membrane, catalytic layer, microporous layer,and GDL.

MEA thickness reduction also agrees to the observed overall fuel cell voltage reduction that has been the highest for the tests operated with pure reactants (MEA 1: 70 μV/h; MEA 2: 195 μV/h but different operation routine). Moreover, the test performed with synthetic reformate/air has shown higher fuel cell voltage reduction (63 μV/h) than the one operated with H_2/air (57 μV/h) in spite of their similar MEA thickness reduction. The lowest degradation rate observed was for MEA 3 operated with H_2/O_2 whose MEA thickness reduction has been the lowest (8 μV/h). On the one hand, degradation rates have been not much different for the long-term tests operated with H_2/air and synthetic reformate/air. On the other hand, the three long-term tests operated with pure reactants have presented quite different degradation rates. This behavior suggests that fuel cell operation with different reactant gases has no intense impact on fuel cell lifetime. However, the fuel cell characterization techniques presented in the following sections may distinguish the processes that may be responsible of fuel cell degradation over time for those tests showing degradation rates higher than 50 μV/h. Moreover, further investigation must be performed about MEAs belonging to different batches but operated at same operation conditions.

Fuel cell performance over time

Figure 3 shows polarization curves performed for the three long-term tests at different operation times. Long-term tests operated with air (Figures 3a,b) show fuel cell performance improvement from BoL (beginning of life, day 0) to day 7 at low and intermediate current densities. Higher current densities than 0.6 A/cm^2 have developed similar fuel cell performance between the two curves. Therefore, the observed fuel cell voltage enhancement in Figures 2a,b, that is, the tests performed with air, could be due to activation of the catalyst and membrane proton conduction improvement. This behavior suggests that removal of impurities from the catalyst, ripening of the catalyst, redistribution of the electrolyte, and membrane humidification have not been completed during the previous break-in procedure yet. After day 7 of operation, the tests from Figures 3a,b have undergone fuel cell voltage reduction in the whole range of current densities until the end of the tests. Thus, the test performed with pure H_2 and air has reduced its voltage 5% in 35 days of test at 0.3 A/cm^2, meanwhile the test performed with synthetic reformate and air has developed voltage reduction of 7% in 36 days of test at 0.3 A/cm^2.

Figure 3c shows the polarization curves over time for the long-term test performed with pure H_2 and O_2 (MEA 1). Opposite to the voltage trend observed for the tests performed with air, this third test has shown fuel cell voltage reduction in the whole range of current densities from BoL until end of the test. Thus, fuel cell voltage at 0.3 A/cm^2 has been reduced by 7% in 21 days of operation. Operation with pure O_2 may accelerate removal of impurities from the catalyst and ripening of the catalyst as well as degradation processes such us carbon corrosion, Pt detachment and/or Pt dissolution/precipitation[32–34] that reduce fuel cell lifetime. Thus, neither fuel cell voltage improvement (Figure 2c) nor fuel cell performance enhancement (Figure 3c) are followed after BoL.

It must be pointed out that the performance of the fuel cell test operated with pure H_2 and O_2 is lower at BoL than the other two tests operated with air but pure O_2 operation may show higher fuel cell performance that air operation. On the one hand, the test performed with pure reactants has been performed using grid flow fields instead of serpentine flow fields as described in the experimental section. This different flow field design might turn into fuel cell performance reduction. Besides, grid flow field design might also cause different compression leading to higher mass transport limitations.[26] Lobato

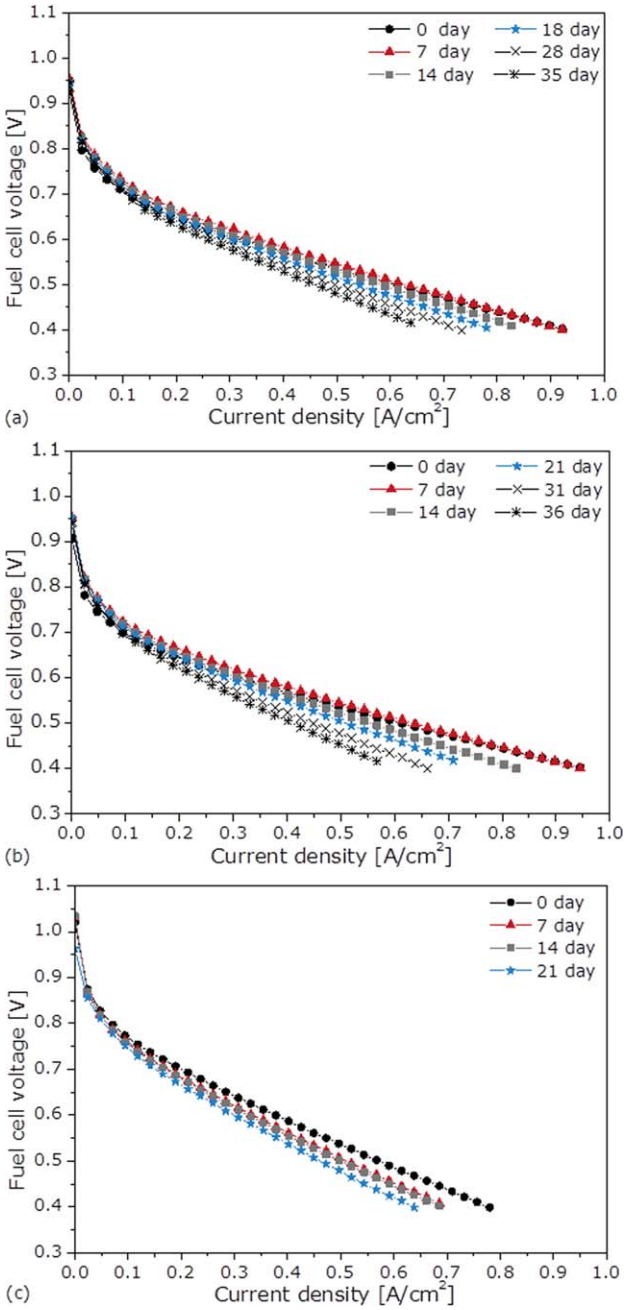

Figure 3. Polarization curves for the fuel cell operating with (a) H_2/air ($\lambda_{anode}/\lambda_{cathode} = 1.5/2$), (b) 78% H_2 + 22% CO_2/air ($\lambda_{anode}/\lambda_{cathode} = 1.5/2$), (c) H_2/O_2 ($\lambda_{anode}/\lambda_{cathode} = 1.5/9.5$) at different operation times.

***T* = 160°C, *p* = 0.1 MPa, (a) and (b) fivefold serpentine and (c) grid flow field, $P_{c,real}$ = 1.4 MPa. [Color figure can be viewed in the online issue, which is available at wileyonlinelibrary.com.]**

et al.[35] observed that the use of serpentine or grid flow fields should not affect the fuel cell performance although slightly higher limiting current densities were predicted when using serpentine geometry. Lobato et al.[36] also reported that current density distribution between grid and serpentine flow fields were similar in a PBI-based HT-PEMFC. On the other hand, Li et al.[37] reported in their review about BBP design for LT-PEMFC application that reactants flowing through grid flow fields tend to follow the path of least resistance across the flow field, which may lead to channeling and the formation of stagnant areas. If such a behavior would happen, lower fuel cell performance could be observed and might also reduce fuel cell lifetime as observed for the test performed with pure reactants. Therefore, the lower fuel cell performance shown by the MEA operated with pure reactants might be due to the manufacturing process of the MEA which is confidential while fuel cell lifetime would be also affected by the different flow field designs used.

Electrochemical impedance spectroscopy

In this section, the impedance spectra are shown for the three long-term tests. Thus, Figure 4 shows Nyquist plots and the equivalent circuits used for each one of the tests. The equivalent circuits have been used for fitting the data from Nyquist plots to better understand the different contributions of the polarization resistance to the general behavior of the fuel cell. In such a way, Figure 5 shows the results from impedance fittings, that is, the different contributions of the polarization resistances, whereas Figure 6 shows the high and intermediate frequency pseudocapacitances for the three long-term tests.

The different elements that form the equivalent circuits can be explained as follows. R_{Ohm} is the resistance of protons and electrons conduction.[38] Besides, this resistance is used to summarize the resistances between wires and MEA contact interfaces.[39,40] In Figure 4, R_{Ohm} is the intersection of the impedance with the real axis at high frequencies. In series with R_{Ohm}, parallel resistor-constant phase element (CPE) pairs are placed to account for each one of the depressed semicircles at high (hf), intermediate (if), and low (lf) frequencies that can be observed in the impedance spectra from Figure 4. CPE are used for modeling double layer capacitance in cases where there are spatial variations in the capacitance to enhance the quality of the fittings curves[41,42] and hence, the CPE_{hf}, CPE_{if}, and CPE_{lf} represent the associated pseudocapacitances to R_{hf}, R_{if}, and R_{lf}, respectively. The CPE impedance is usually given by Eq. 1

$$Z_{CPE} = Q^{-1} \cdot (i\omega)^{-n} \tag{1}$$

where Q is the pseudocapacitance, $i = \sqrt{-1}$, ω is the frequency and n is the CPE exponent that characterizes the phase shift. The impedance represents a resistor for $n = 0$, a capacitor for $n = 1$ and a coil for $n = -1$. For $0.8 < n < 1$, the CPE corresponds to distortion of the capacitance due to electrode surface roughness or distribution/accumulation of charge carriers. Thus, CPE is a generalized element that can be connected to electrode surface roughness, thickness or composition, nonuniform current distribution and inhomogeneous reaction rates on the electrode surface.[38] For Nyquist plots fittings, the exponents for CPE_{hf} and CPE_{if} have been fixed at 0.85, while the exponent for CPE_{lf} has been fixed at 1.[43] The exponents have been kept constant to improve the fit and to avoid randomly resistance trends.[23,42] Therefore, the pseudocapacitive elements at high and intermediate frequencies account to electrode surface roughness or distribution/accumulation of charge carriers as reported above, whereas the element at low frequencies account to pure charge carriers storage in the porous structure of the GDL and electrodes because of free electrons available from the electrochemical reactions.[24,44]

R_{hf} is represented by the diameter of the arc at high frequencies. The high frequency arc is recognized as potential

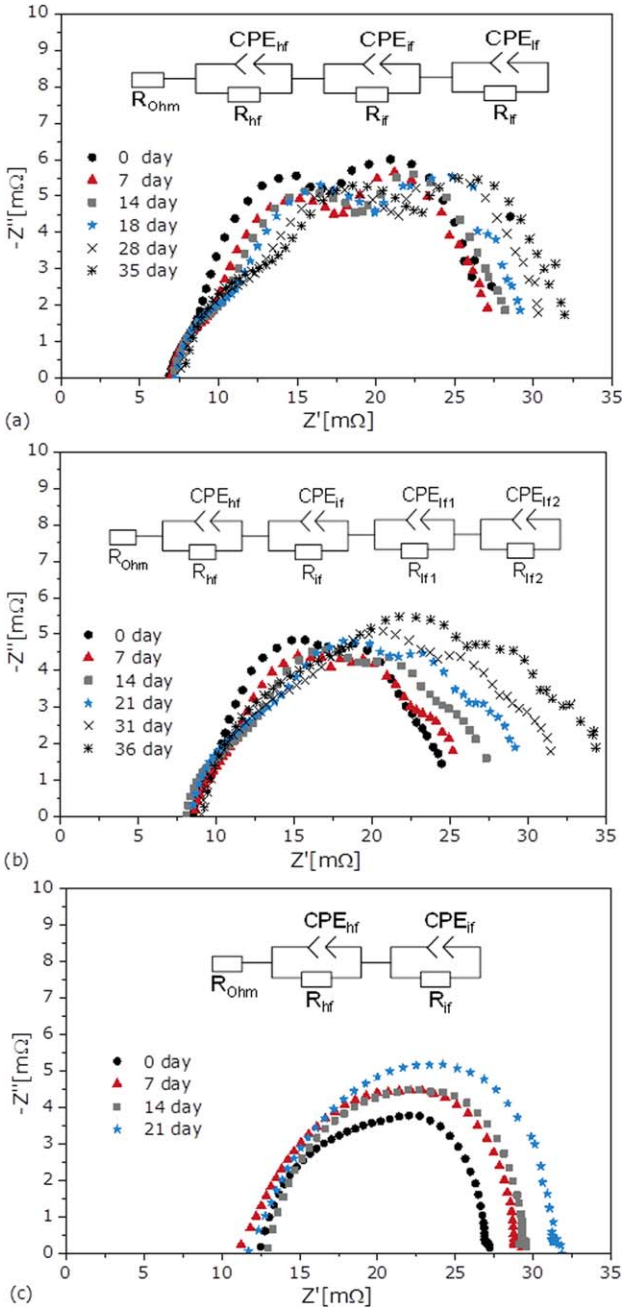

Figure 4. Impedance spectra at 0.3 A/cm^2 and equivalent circuits for the fuel cell operating with (a) H_2/air ($\lambda_{anode}/\lambda_{cathode} = 1.5/2$), (b) 78% H_2 + 22% CO_2/air ($\lambda_{anode}/\lambda_{cathode} = 1.5/2$), (c) H_2/O_2 ($\lambda_{anode}/\lambda_{cathode} = 1.5/9.5$) at different operation times.

***T* = 160°C, *p* = 0.1 MPa, (a) and (b) fivefold serpentine and (c) grid flow field, $P_{c,real}$ = 1.4 MPa. [Color figure can be viewed in the online issue, which is available at wileyonlinelibrary.com.]**

independent[45] but authors attributed the arc to resistance effects in the electrolyte within the catalyst layer[45–47] and/or to anode charge transfer resistance (hydrogen oxidation reaction, HOR, activation losses).[40,43] R_{if} is the diameter of the arc at intermediate frequencies and it is the cathode charge transfer resistance (ORR activation losses).[23] R_{lf} is the resistance related to the arc at low frequencies. At low frequencies, the contribution to the impedance of gas (H_2, CO_2, air, and H_2O) diffusion processes is acquired.[48]

In this work, different reactant gases concentrations have been used and hence, mass transfer limitations are different between each one of the performed tests. Thus, the equivalent circuit used in the test performed with pure H_2 and air includes

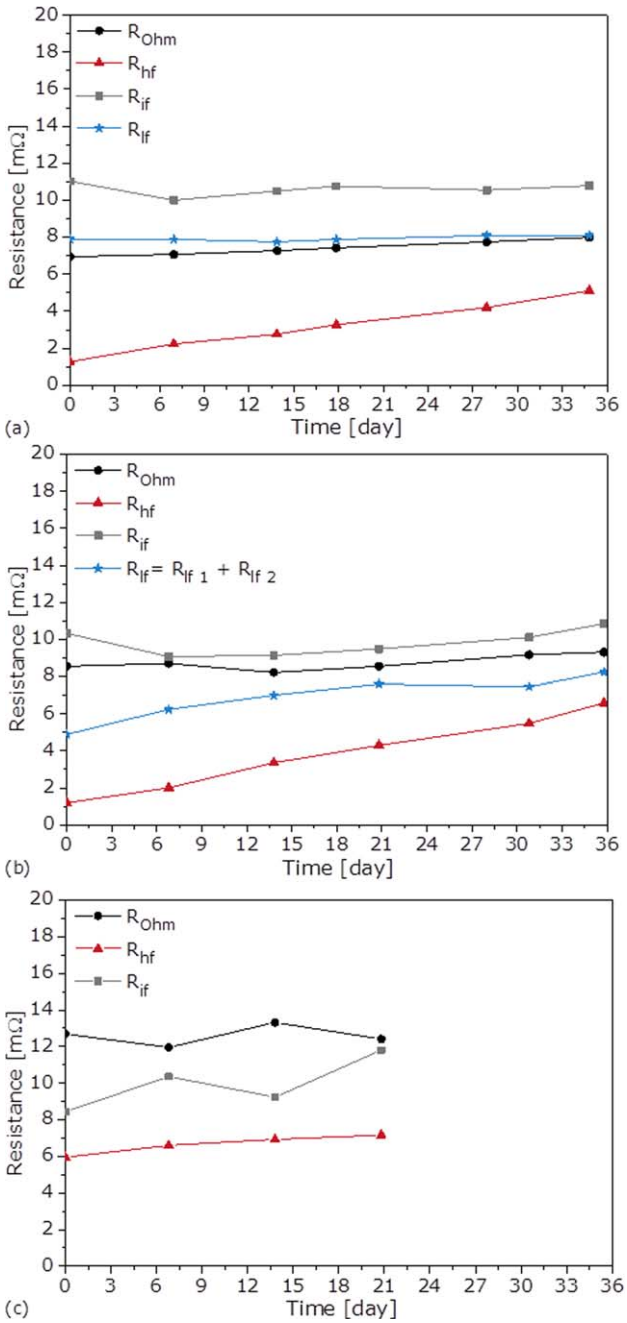

Figure 5. Ohmic, high, intermediate, and low frequency resistances from fittings of Nyquist plots at 0.3 A/cm^2 (Figure 4) for the fuel cell operating with (a) H_2/air ($\lambda_{anode}/\lambda_{cathode} = 1.5/2$), (b) 78% H_2 + 22% CO_2/air ($\lambda_{anode}/\lambda_{cathode} = 1.5/2$), (c) H_2/O_2 ($\lambda_{anode}/\lambda_{cathode} = 1.5/9.5$) at different operation times.

***T* = 160°C, *p* = 0.1 MPa, (a) and (b) fivefold serpentine and (c) grid flow field, $P_{c,real}$ = 1.4 MPa. [Color figure can be viewed in the online issue, which is available at wileyonlinelibrary.com.]**

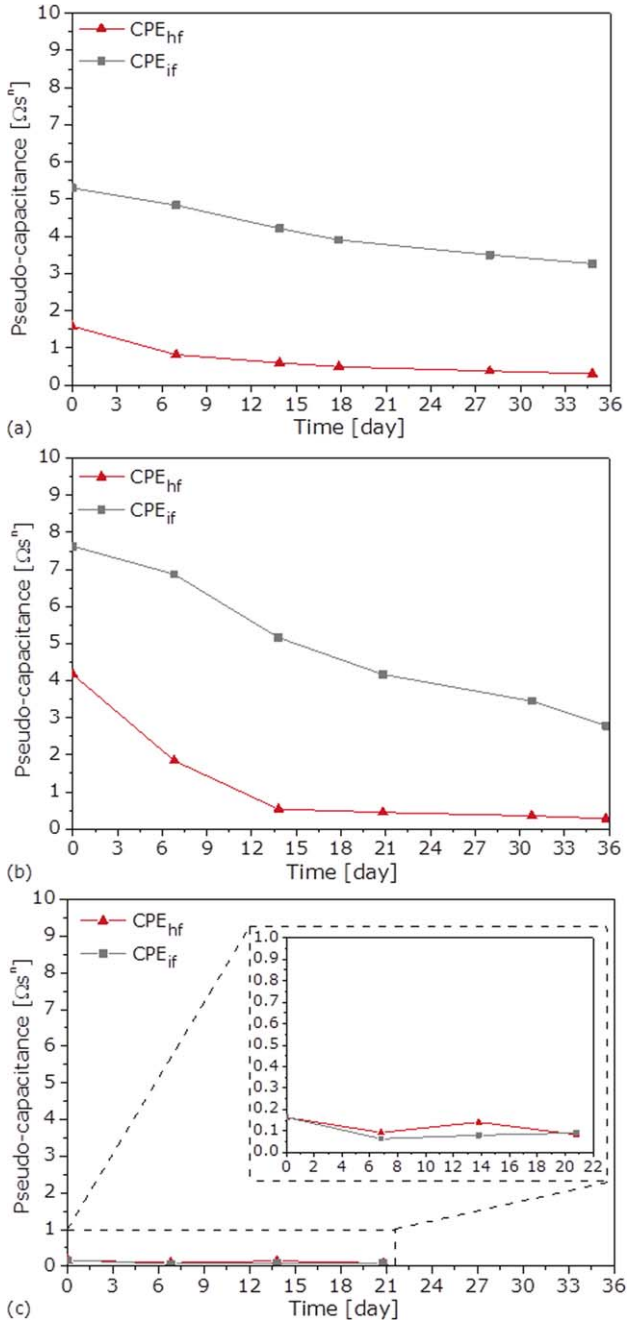

Figure 6. High and intermediate frequency pseudocapacitances from fittings of Nyquist plots at 0.3 A/cm^2 (Figure 4) for the fuel cell operating with (a) H_2/air ($\lambda_{anode}/\lambda_{cathode} = 1.5/2$), (b) 78% H_2 + 22% CO_2/air ($\lambda_{anode}/\lambda_{cathode} = 1.5/2$), (c) H_2/O_2 ($\lambda_{anode}/\lambda_{cathode} = 1.5/9.5$) at different operation times.

***T* = 160°C, *p* = 0.1 MPa, (a) and (b) fivefold serpentine and (c) grid flow field, $P_{c,real}$ = 1.4 MPa. [Color figure can be viewed in the online issue, which is available at wileyonlinelibrary.com.]**

one resistor-CPE pair for the low frequency range as anode mass transfer limitations are minimized due to the use of pure H_2, so the main contribution to the low frequency resistance in Figure 4a is cathode mass transfer. In case of the test performed with synthetic reformate and air, the equivalent circuit includes two resistor-CPE pairs for the low frequency range as four capacitive loops are observed in the Nyquist plots from Figure 4b. For the third test performed with pure H_2 and O_2, mass transfer in both cathode and anode are minimized due to the use of pure reactants so the equivalent circuit may be simplified without taking into account mass transfer losses and two capacitive loops are also observed (Figure 4c). Moreover, the resistance associated with low frequency in Figure 5b is represented as the sum of both the R_{lf1} and the R_{lf2}. Further investigations must be done by the authors before dealing with the two low frequency resistances separately.

R_{Ohm} has shown a weak increase over time for the tests performed with pure H_2/air (Figure 5a) and synthetic reformate/air (Figure 5b). Moreover, the resistance has undergone an increase of +0.9 mΩ over 1000 h of operation in the two tests. Therefore, the membrane electrolyte may develop a weak reduction of proton conductivity over time. From Figure 5c, R_{Ohm} has not shown a clear increasing trend during the 21 days of operation for the test performed with pure reactants. In addition, this trend could also not be clearly identified for the test performed with synthetic reformate/air in the day 21 of operation. Thus, longer operation times than 1000 h of operation at constant load are required to better identify the ohmic losses. It can be also observed that R_{Ohm} values from the test performed with pure reactants are higher than the ones from the other two tests. This behavior could be owing to lower proton conductivity of the MEA operated with H_2/O_2. Moreover, lower proton conductivity insinuates lower electrolyte content in the MEA than in the other MEAs tested with H_2/air and synthetic reformate/air.

In the case of R_{hf}, trends can be better identified than R_{Ohm} from BoL to the end of the three tests. In Figure 5a, R_{hf} has raised +3.8 mΩ over the whole test. Worse HOR kinetics over time may be responsible for the R_{hf} increase so anode catalyst deterioration has been discerned over time. As mentioned previously, R_{hf} is also related to proton conduction in catalyst layer, in such a way, the slight increase on R_{Ohm} influences the R_{hf} increase over time as well. The test performed with synthetic reformate/air (Figure 5b) has developed higher tilting in R_{hf} than the test performed with pure H_2/air. R_{hf} has raised +5.4 mΩ from BoL until the end of the test. Andreasen et al.[23] reported increase in the R_{hf} when 25% CO_2 was added in the fuel inlet during their investigations with a PBI-based HT-PEMFC. Besides, Boillot et al.[18] also reported that the high frequency loop was strongly dependent on the H_2 dilution rate. So dilution of the H_2 stream with CO_2 could lead to fuel starvation of some regions of the anode catalyst layer that turns into faster anode catalyst deterioration over time.

Moreover, CO_2 may generate small amounts of CO by the reversed water gas shift reaction (RWGS) that could poison the anode catalyst over time. Formation of CO through RWGS, with the subsequent poisoning of the Pt catalyst on the anode electrode has already been quantified in literature for LT-PEMFC.[49,50] Das et al.[51] compared the performance of a HT-PEMFC with CO concentrations from 2 to 5% in the fuel at operation temperatures from 140 to 180°C. A cell diagnostic test showed that CO can be tolerated at current densities less than 0.3 A/cm^2 with fuel cell voltage higher than 0.5 V at 180°C. Besides, the results suggested that the CO effect on voltage loss would be negligible operating the PEMFC at 180°C or above in that CO concentration range as Pt surface coverage by CO at high temperature is very low compared to lower temperatures. R_{hf} from Figure 5c has shown lesser tilting trend than the one observed in Figure 5a. Thus, R_{hf} has increased +1.2 mΩ in 21 days of operation for the test

performed with pure H_2/O_2 and +2.0 mΩ in the first 21 days of operation for the test performed with pure H_2/air. In a first hypothesis, higher oxygen partial pressure could enhance longevity of anode catalyst. Operating with pure O_2, cathode catalyst utilization ORR rates increases.[52] In PEMFC, the ORR is the sluggish reaction so that ORR kinetics enhancement would also enhance HOR kinetics that may turn into higher anode catalyst utilization as well. Improving anode catalyst utilization for the HOR may reduce catalyst sites availability for side reactions. Nevertheless, further investigations must be done to understand better this behavior. In contrast, R_{hf} values for the fuel cell operated with pure reactants have been higher than those for the other two presented long-term tests. Thereby, these high R_{hf} values may be influenced by R_{Ohm} as reported above so lower membrane proton conductivity may lead to lower proton conductivity in catalyst layer as well. However, anode charge transfer is also part of R_{hf} that suggests worse anode catalyst operation than for the other tests.

Intermediate frequency resistance, R_{if}, from Figures 5a,b has shown a reduction from beginning to day 7 of the tests operated with air, meanwhile R_{if} from Figure 5c has presented an increasing trend over the whole period of the test (+5.9 mΩ). On the one hand, R_{if} increase over time from Figure 5c agrees to the observations from Figure 3c due to cathode catalyst degradation. On the other hand, fuel cell performance improvement observed in Figures 3a,b may be due to improvement of the ORR kinetics. This behavior suggests that the break-in procedure duration must be extended for fuel cell operation with air. Therefore, cathode catalyst degradation has taken place from day 7 until the end of the tests performed with air as oxidant. Besides, R_{if} increase from Figure 5a has been nearly imperceptible as it has increased +0.8 mΩ from day 7 till day 35 so longer operation times are required to better identify the cathode charge transfer losses. In the case of Figure 5b, R_{if} has increased +1.8 mΩ from day 7 till day 36 and hence, operation with synthetic reformate/air also has developed a higher degradation of cathode catalyst compared to operation with pure H_2/air. Thus, cathode catalyst degradation is influenced by anode catalyst degradation as well.

The contribution of gas diffusion processes to the impedance, R_{lf}, has been rather stable in Figure 5a during the whole test. Therefore, porosity and hydrophobicity properties of the carbon GDEs may remain in a steady state. On contrary, R_{lf} from Figure 5b has displayed an increasing trend over time (+3.4 mΩ). Therefore, fuel cell operation with the synthetic reformate has worsened gases mass transfer rates over time. Meland et al.[53] studied the influence of CO poisoning of the anode in a LT-PEMFC using EIS. They concluded that CO adsorbs to the porous carbon matrix, and reduces significantly the rate of surface diffusion of hydrogen to the surface. Thus, the assumption that CO may be present in the anode due to RWGS reaction is favoured. Therefore, the mass transfer limitations increase may be the consequence of an accumulative effect of CO within the porous structure of the GDE so further investigations would be focused on detection and quantification of CO. A recent publication from Eberhardt et al.[54] has shown electrolyte migration from cathode to anode during fuel cell testing. Besides, it was demonstrated that the migration and consequently gas diffusion layer flooding of the anode occurred, and hence this process was almost reversible as phosphoric acid droplets were in the GDL and flow fields after returning the current density from high to low values. Consequently, the synthetic reformate/air test may be also influenced by phosphoric acid saturation in the GDL that may worsen mass transport owing to the reduced hydrogen partial pressure. Moreover, anode catalyst can be also poisoned by phosphate ions adsorption as a consequence of electrolyte migration so the observed R_{hf} increase in the three long term tests may be also connected to this process. Last but not least, each load cycle performed during MEA characterization lead to electrolyte loss for the long-term tests studied that should also influence fuel cell performance after MEA characterization as discussed above.

In Figures 6a,b, the high frequency pseudocapacitance between the MEA operated with H_2/air and the one operated with synthetic reformate/air have similar values so that anode electrodes have been similarly active to HOR.[18] Similar discussion can be drawn for the intermediate pseudocapacitance so cathode electrodes have been similarly active to ORR. The MEA operated with pure reactants (Figure 6c) has shown rather low pseudocapacitances and they have evolved differently to the previous two long-term tests, thereby anode and cathode electrodes are probably less active in comparison with the other two MEAs to HOR and ORR, respectively. Boillot et al.[18] reported anode pseudocapacitance 10 times lower than that of the cathode in one MEA whereas the second MEA used in their investigations showed no significant difference in anode and cathode pseudocapacitances. Then, it was considered that the electrodes were not symmetrical and one of the electrodes was probably less active than the other. Thus, the lower performance shown by the MEA operated with pure reactants may be to less catalyst activity of the MEA electrodes as discussed above. On the contrary, Kondratenko et al.[55] reported that oxidant switch from oxygen to air turned to increase capacitance values and may be ascribed to the fact that the measured capacitance contained both double layer and mass transport capacitances contributions. On the one hand, the evolution in time of the pseudocapacitances values from Figures 6a,b has shown that they have been reduced over time. High frequency values have reached an asymptote after almost 15 days of operation, while intermediate frequency values have been not. On the other hand, Figure 6c has shown almost constant values over the whole test. In case of pseudocapacitance would contribute to mass transport from electrolyte components onto catalyst surface, it must be said that the MEA operated with pure reactants have shown well mass transport during the whole test, meanwhile mass transport in the catalyst layer has been improved for the other two tested MEAs over time due to redistribution of electrolyte throughout the whole catalyst surface area. Nevertheless, further investigations must be done to better understand the influence of the CPE parameters and how they evolve over time in a HT-PEMFC.

Linear sweep voltammetry

Linear sweep voltammetries are shown in Figure 7 for the three long term tests. This figure collects the LSV measurements at BoL and end of the tests. From Figures 7a,b, changes in the slope of the LSV during time have been negligible, so internal resistance over time remains in a steady state. That means membrane thinning has not occurred during the operation with pure H_2/air or synthetic reformate/air in 1000 h of operation. Different observations can be drawn from Figure 7c (H_2/O_2). MEA 1 has shown increase of the LSV slope as well as current density values in the whole range of potential of the voltammogram from beginning to end of the test. In this case, short circuit as well as hydrogen crossover rates have become larger during operation owing to the degradation of the

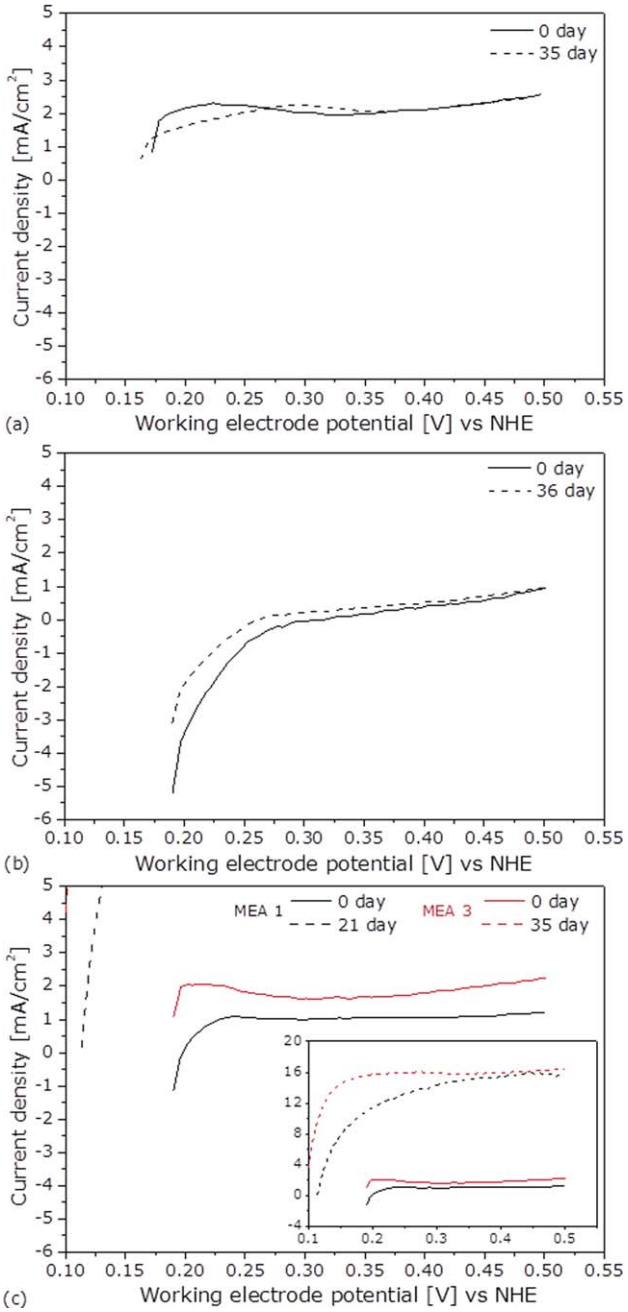

Figure 7. Linear sweep voltammetries at the beginning and the end of the long-term tests for the fuel cell operating with (a) H_2/air, (b) 78% H_2 + 22% CO_2/air and (c) H_2/O_2.

$T = 160°C$, $p = 0.1$ MPa, fivefold serpentine and grid flow field (MEA 1 in c), $P_{c,real} = 1.4$ MPa. Flow rates: $H_2/N_2 = 0.3/0.3$ L/min, scan rate = 2 mV/s. [Color figure can be viewed in the online issue, which is available at wileyonlinelibrary.com.]

membrane electrolyte. Different causes may be the reason of membrane degradation during time due to exposure at high oxygen concentrations, such us membrane thinning and pinhole growth by chemical degradation[5] or carbon fibers intrusion from one electrode to another.[27] Thus, the huge voltage drop observed in Figure 2c after 21 days of operation must be due to catalyst deterioration and mainly internal short circuit formation as well as hydrogen crossover from anode to cathode sides that have turned into the considerable reduction of the fuel cell electrical efficiency. LSV at BoL and end of test for the previously shown MEA 3 operated with pure reactant have been also included in Figure 7c to show that hydrogen crossover increase due to pure oxygen operation is not an isolated result. MEA 3 has shown slightly higher currents than MEA 1 at BoL as well as more sloping voltammogram that suggest higher hydrogen crossover and internal resistance. After 35 days of operation, MEA 3 voltammogram has displayed current density increase in the whole range of swept potential reaching similar values than MEA 1 at end of life although slope is similar to the one recorded at BoL. Thus, hydrogen crossover increase has not been displayed with a substantial short circuit formation that suggests chemical degradation of membrane owing to thinning and/or pinhole growth but not fibers intrusion from one electrode to another.

Conclusions

The effects of operating commercial PBI-based HT-PEM MEAs with different reactant gases have been electrochemically investigated in 1000 h long-term tests at constant current density conditions. Fuel cell operation with air as oxidant suggests the need of a longer break-in procedure. Operation with pure H_2 and air also requires longer investigating times to identify the different degradation mechanisms in the membrane and cathode catalyst sides. Operating the fuel cell with a CO_2 and H_2 fuel mixture leads to faster degradation of anode catalyst that may influence cathode catalyst degradation and deployment of mass transportation in the anode GDE over time. Thus, identification and quantification of CO generation from CO_2 via RWGS reaction as well as phosphoric acid redistribution in GDE must be performed in further investigations at the fuel cell operation conditions. How anode degradation may influence cathode catalyst degradation in PBI-based HT-PEMFCs needs also to be answered in the future. Nevertheless, fuel cell operation with hydrogen and carbon dioxide mixture has no intense impact on fuel cell lifetime in comparison to operating with pure hydrogen. A fuel cell operated with pure H_2 and O_2 accelerates degradation of MEA components such as the cathode catalyst and membrane electrolyte although grid flow field geometry used in BBP instead of serpentine one could also influence MEA longevity. However, pure oxygen operation mode must be further investigated to deal with the different degradation rates observed. MEA characterization used techniques influence negatively fuel cell durability as the cathode potential is cycled several times so electrolyte migration and catalyst deterioration have been enhanced.

Further investigations in the studied MEAs must be accomplished in a post-mortem analysis by means of imaging techniques to better distinguish degradation mechanisms in the MEA materials. The results will be shown in future publications.

Acknowledgments

The authors would like to thank Stefanie Laue who did an excellent job in the laboratories to gather the data for this publication.

We would also like to thank the European Commission for supporting this work by the Fuel Cells and Hydrogen Joint Undertaking as this work was supported by the Seventh Framework Program through the project CISTEM (Grant Agreement Number 325262) and the company Danish Power Systems for providing MEAs.

Notation

BoL = beginning of life
BPP = bipolar plate
CCU = cell compression unit
CHP = combined heat and power
CISTEM = construction of improved HT-PEM MEAs and stacks for long term stable modular CHP unit
CL = catalytic layer
CPE = constant phase element
DPS = Danish Power Systems
EIS = electrochemical impedance spectroscopy
FCH-JU = fuel cell and hydrogen joint undertaking
GDE = gas diffusion electrode
GDL = gas diffusion layer
hf = high frequency
HOR = hydrogen oxidation reaction
HT-PEM = high temperature polymer electrolyte membrane
if = intermediate frequency
lf = low frequency
LSV = linear sweep voltammetry
LT-PEM = low temperature polymer electrolyte membrane
MEA = membrane electrode assembly
MPL = micro porous layer
n = CPE exponent
NHE = normal hydrogen electrode
OCV = Open Circuit Voltage
Ohm = ohmic
ORR = oxygen reduction reaction
p = pressure of the fuel cell
PBI = polybenzimidazole
P_c = MEA contact pressure
PEMFC = polymer electrolyte membrane fuel cell
Q = CPE pseudocapacitance
R = resistance
RWGS = reverse water gas shift
λ = stoichiometric factor
ω = frequency

Literature Cited

1. Korsgaard AR, Nielsen MP, Kaer SK. Part one: a novel model of HTPEM-based micro-combined heat and power fuel cell system. *Int J Hydrogen Energy*. 2008;33(7):1909–1920.
2. Karstedt J, Ogrzewalla J, Severin C, Pischinger S. Development and design of experiments optimization of a high temperature proton exchange membrane fuel cell auxiliary power unit with onboard fuel processor. *J Power Sources*. 2011;196:9998–10009.
3. Mishra AK, Bose S, Kuila T, Kim NH, Lee JH. Silicate-based polymer-nanocomposite membranes for polymer electrolyte membrane fuel cells. *Prog Polym Sci*. 2012;37(6):842–869.
4. Seel DC, Benicewicz BC, Xiao L, Schmidt TJ. High-temperature polybenzimidazole-based membranes. In: Vielstich W, Gasteiger HA, Yokokawa H, editors. *Handbook of Fuel Cells: Fundamentals, Technology and Applications, Vol. 5*. Wiley, 2009:300–312.
5. Mader J, Xiao L, Schmidt TJ, Benicewicz BC. Polybenzimidazole/acid complexes as high-temperature membranes. *Adv Polym Sci*. 2008;216:63–124.
6. Li Q, He R, Gao J-A, Jensen JO, Bjerrum NJ. The CO poisoning effect in PEMFCs operational at temperatures up to 200 DegC. *J Electrochem Soc*. 2003;150(12):A1599–A1605.
7. Lobato J, Canizares P, Rodrigo MA, Linares JJ. PBI-based polymer electrolyte membranes fuel cells: temperature effects on cell performance and catalyst stability. *Electrochim Acta*. 2007;52:3910–3920.
8. Lobato J, Canizares P, Rodrigo MA, Ubeda D, Pinar FJ. Enhancement of the fuel cell performance of a high temperature proton exchange membrane fuel cell running with titanium composite polybenzimidazole-based membranes. *J Power Sources*. 2011;196(20):8265–8271.
9. Ma YL, Wainright JS, Litt MH, Savinell RF. Conductivity of PBI membranes for high-temperature polymer electrolyte fuel cells. *J Electrochem Soc*. 2004;151(1):A8–A16.
10. Li Q, He R, Jensen JO, Bjerrum NJ. Approaches and recent development of polymer electrolyte membranes for fuel cells operating above 100°C. *Chem Mater*. 2003;15:4896–4915.
11. Wilkinson DP, St-Pierre J. Durability. In: Vielstich W, Gasteiger HA, Lamm A, editors. *Handbook of Fuel Cells: Fundamentals, Technology and Applications, Vol. 3*. Wiley, 2003:611–626.
12. Borup R, Meyers J, Pivovar B, Kim YS, Mukundan R, Garland N, Myers D, Wilson M, Garzon F, Wood D, Zelenay P, More K, Stroh K, Zawodzinski T, Boncella J, McGrath JE, Inaba M, Miyatake K, Hori M, Ota K, Ogumi Z, Miyata S, Nishikata A, Siroma Z, Uchimoto Y, Yasuda K, Kimijima K, Iwashita N. Scientific aspects of polymer electrolyte fuel cell durability and degradation. *Chem Rev*. 2007;107(10):3904–3951.
13. Wu J, Yuan XZ, Martin JJ, Wang H, Zhang J, Shen J, Wu S, Merida W. A review of PEM fuel cell durability: degradation mechanisms and mitigation strategies. *J Power Sources*. 2008;184(1):104–119.
14. Schmidt TJ. Durability and dregradation in high-temperature polymer electrolyte fuel cells. *ECS Trans*. 2006;1(8):19–31.
15. Oono Y, Sounai A, Hori M. Long-term cell degradation mechanism in high-temperature proton exchange membrane fuel cells. *J Power Sources*. 2012;210(0):366–373.
16. Yu S, Xiao L, Benicewicz BC. Durability studies of PBI-based high temperature PEMFCs. *Fuel Cells (Weinheim, Germany)*. 2008;8(3–4):165–174.
17. Chang WR, Hwang JJ, Weng FB, Chan SH. Effect of clamping pressure on the performance of a PEM fuel cell. *J Power Sources*. 2007;166:149–154.
18. Boillot M, Bonnet C, Jatroudakis N, Carre P, Didierjean S, Lapicque F. Effect of gas dilution on PEM fuel cell performance and impedance response. *Fuel Cells*. 2006;6(1):31–37.
19. Jalani NH, Ramani M, Ohlsson K, Buelte S, Pacifico G, Pollard R, Staudt R, Datta R. Performance analysis and impedance spectral signatures of high temperature PBI-phosphoric acid gel membrane fuel cells. *J Power Sources*. 2006;160(2):1096–1103.
20. Travassos MA, Rangel CM. Polarity reversal in PEM fuel cells by fuel starvation. *3° Seminário Internacional Torres Vedras: Hydrogen Energy and Sustainability: Advances in Fuel Cells and Hydrogen Workshop*. Portugal: Associação Portuguesa para a Promoção do Hidrogénio (Portuguese Association for the Promotion of Hydrogen) 2010:48–52.
21. de Bruijn FA, Dam VAT, Janssen GJM. Review: durability and degradation issues of PEM Fuel Cell components. *Fuel Cells (Weinheim, Germany)*. 2008;8(1):3–22.
22. Scholta J, Pawlik J, Chmielewski N, Jörissen L. Longevity test results for reformate polymer electrolyte membrane fuel cell stacks. *J Power Sources*. 2011;196(12):5264–5271.
23. Andreasen SJ, Vang JR, Kaer SK. High temperature PEM fuel cell performance characterisation with CO and CO2 using electrochemical impedance spectroscopy. *Int J Hydrogen Energy*. 2011;36(16):9815–9830.
24. Jespersen JL, Schaltz E, Kaer SK. Electrochemical characterization of a polybenzimidazole-based high temperature proton exchange membrane unit cell. *J Power Sources*. 2009;191(2):289–296.
25. Diedrichs A, Wagner P. Performance analysis of a high-temperature polymer electrolyte membrane fuel cell under mechanical compression control. *ECS Trans*. 2012;50(2):1137–1153.
26. Diedrichs A, Rastedt M, Pinar JF, Wagner P. Effect of compression on the performance of a HT-PEM fuel cell. *J Appl Electrochem*. 2013;43(11):1079–1099.
27. Pinar FJ, Rastedt M, Pilinski N, Wagner P. Effect of compression cycling on polybenzimidazole-based high-temperature polymer electrolyte membrane fuel cells. *Fuel Cells*. 2015;15(1):140–149.
28. Tingeloef T, Ihonen JK. A rapid break-in procedure for PBI fuel cells. *Int J Hydrogen Energy*. 2009;34(15):6452–6456.
29. Pinar FJ, Canizares P, Rodrigo MA, Ubeda D, Lobato J. Scale-up of a high temperature polymer electrolyte membrane fuel cell based on polybenzimidazole. *J Power Sources*. 2011;196(9):4306–4313.
30. Darling RM, Meyers JP. Kinetic model of platinum dissolution in PEMFCs. *J Electrochem Soc*. 2003;150(11):A1523–A1527.
31. Jahnke T, Latz A. Modeling reversible and irreversible degradation in direct methanol fuel cells. In: *5th European PEFC and H2 Forum*. Lucerne, 2015.
32. Dokiya M, Fuller TF, Hamnett A, Iwasita T, Kordesch K, LaConti AB, Sandstede G, Scherer GG, Selman JR, Yokokawa H. *Fuel Cell Technology and Applications: Part 1, Vol. 3*. Wiley-VCH, 2003.
33. Zhai Y, Zhang H, Liu G, Hu J, Yi B. Degradation study on MEA in H3PO4/PBI high-temperature PEMFC life test. *J Electrochem Soc*. 2007;154(1):B72–B76.
34. Hu J, Zhang H, Zhai Y, Liu G, Hu J, Yi B. Performance degradation studies on PBI/H3PO4 high temperature PEMFC and one-dimensional numerical analysis. *Electrochim Acta*. 2006;52(2):394–401.
35. Lobato J, Canizares P, Rodrigo MA, Pinar FJ, Mena E, Ubeda D. Three-dimensional model of a 50 cm^2 high temperature PEM fuel

cell. Study of the flow channel geometry influence. *Int J Hydrogen Energy*. 2010;35(11):5510–5520.
36. Lobato J, Canizares P, Rodrigo MA, Pinar FJ, Ubeda D. Study of flow channel geometry using current distribution measurement in a high temperature polymer electrolyte membrane fuel cell. *J Power Sources*. 2011;196(9):4209–4217.
37. Li X, Sabir I. Review of bipolar plates in PEM fuel cells: flow-field designs. *Int J Hydrogen Energy*. 2005;30(4):359–371.
38. Yuan X-Z, Song C, Wang H, Zhang J. *Electrochemical Impedance Spectroscopy in PEM Fuel Cells: Fundamentals and Applications*, 1st ed. London: Springer, 2010.
39. Chen C-Y, Lai W-H. Effects of temperature and humidity on the cell performance and resistance of a phosphoric acid doped polybenzimidazole fuel cell. *J Power Sources*. 2010;195:7152–7159.
40. Andreasen SJ, Jespersen JL, Schaltz E, Kær SK. Characterisation and modelling of a high temperature PEM fuel cell stack using electrochemical impedance spectroscopy. *Fuel Cells*. 2009;4:463–473.
41. Andreasen SJ, Mosbæk R, Vang JR, Kær SK, Araya SS. EIS characterization of the poisoning effects of CO and CO_2 on a PBI based HT-PEM fuel cell. In: *ASME 2010 Eighth International Fuel Cell Science, Engineering and Technology Conference*. New York, 2010.
42. Mainka J, Maranzana G, Dillet J, Didierjean S, Lottin O. On the estimation of high frequency parameters of Proton Exchange Membrane Fuel Cells via Electrochemical Impedance Spectroscopy. *J Power Sources*. 2014;253:381–391.
43. Wagner N. Characterization of membrane electrode assemblies in polymer electrolyte fuel cells using a.c. impedance spectroscopy. *J Appl Electrochem*. 2002;32(8):859–863.
44. Andreasen SJ, Jespersen JL, Schaltz E, Kaer SK. Characterization and modelling of a high temperature PEM fuel cell stack using electrochemical impedance spectroscopy. *Fuel Cells (Weinheim, Germany)*. 2009;9(4):463–473.
45. Yuan X, Wang H, Sun JC, Zhang J. AC impedance technique in PEM fuel cell diagnosis-A review. *Int J Hydrogen Energy*. 2007; 32(17):4365–4380.
46. Paganin VA, Oliveira CLF, Ticianelli EA, Springer TE, Gonzalez ER. Modelistic interpretation of the impedance response of a polymer electrolyte fuel cell. *Electrochim Acta*. 1998;43(24):3761–3766.
47. Springer TE, Zawodzinski TA, Wilson MS, Gottesfeld S. Characterization of polymer electrolyte fuel cells using AC impedance spectroscopy. *J Electrochem Soc*. 1996;143(2):587–598.
48. Zhang J, Tang Y, Song C, Zhang J. Polybenzimidazole-membrane-based PEM fuel cell in the temperature range of 120-200°C. *J Power Sources*. 2007;172(1):163–171.
49. Gu T, Lee W-K, van Zee JW. Quantifying the 'reverse water gas shift' reaction inside a PEM fuel cell. *Appl Catal B Environ*. 2005; 56:43–49.
50. de Bruijn FA, Papageorgopoulos DC, Sitters EF, Janssen GJM. The influence of carbon dioxide on PEM fuel cell anodes. *J Power Sources*. 2002;110(1):117–124.
51. Das SK, Reis A, Berry KJ. Experimental evaluation of CO poisoning on the performance of a high temperature proton exchange membrane fuel cell. *J Power Sources*. 2009;193:691–698.
52. Benziger J, Kimball E, Mejia-Ariza R, Kevrekidis I. Oxygen mass transport limitations at the cathode of polymer electrolyte membrane fuel cells. *AIChE J*. 2011;57(9):2505–2517.
53. Meland A-K, Kjelstrup S. Three steps in the anode reaction of the polymer electrolyte membrane fuel cell. Effect of CO. *J Electroanal Chem*. 2007;610(2):171–178.
54. Eberhardt SH, Toulec M, Marone F, Stampanoni M, Büchi FN, Schmidt TJ. Dynamic operation of HT-PEFC: in-operando imaging of phosphoric acid profiles and (re)distribution. *J Electrochem Soc*. 2015;162(3):F310–F316.
55. Kondratenko MS, Gallyamov MO, Khokhlov AR. Performance of high temperature fuel cells with different types of PBI membranes as analysed by impedance spectroscopy. *Int J Hydrogen Energy*. 2012;37(3):2596–2602.

Manuscript received Dec. 17, 2014, and revision received July 22, 2015.